Modeling of the cubic and antiferrodistortive phases of $SrTiO_3$ with screened hybrid density functional theory

Fedwa El-Mellouhi,[1,*] Edward N. Brothers,[1,†] Melissa J. Lucero,[2] and Gustavo E. Scuseria[2,3,4]

[1]*Science Program, Texas A&M University at Qatar, Texas A&M Engineering Building, Education City, Doha, Qatar*

[2]*Department of Chemistry, Rice University, Houston, Texas 77005-1892, USA*

[3]*Department of Physics and Astronomy, Rice University, Houston, Texas 77005-1892, USA*

[4]*Chemistry Department, Faculty of Science, King Abdulaziz University, Jeddah 21589, Saudi Arabia*

(Received 17 May 2011; revised manuscript received 8 August 2011; published 20 September 2011)

We have calculated the properties of $SrTiO_3$ (STO) using a wide array of density functionals ranging from standard semilocal functionals to modern range-separated hybrids, combined with several basis sets of varying size and quality. We show how these combinations' predictive ability varies significantly, for both STO's cubic and antiferrodistortive (AFD) phases, with the greatest variation in functional and basis set efficacy seen in modeling the AFD phase. The screened hybrid functionals we utilized predict the structural properties of both phases in very good agreement with experiment, especially if used with large (but still computationally tractable) basis sets. The most accurate results presented in this study, namely, those from HSE06 with a modified def2-TZVP basis set, stand as one of the most accurate modelings of STO to date when compared to the literature; these results agree well with experimental structural and electronic properties as well as providing insight into the band structure alteration during the phase transition.

DOI: 10.1103/PhysRevB.84.115122 PACS number(s): 71.15.Ap, 77.80.−e, 77.84.−s

I. INTRODUCTION

Strontium titanate ($SrTiO_3$; STO) is a complex oxide perovskite of great technological interest for its superconductivity,[1] blue-light emission,[2] photovoltaic effect,[3] and so on. Under normal conditions, bulk $SrTiO_3$ crystallizes in a cubic perovskite structure; it subsequently undergoes a second-order phase transition at $T_c = 105$ K to a tetragonal structure with slightly rotated oxygens around the z axis, known as the antiferrodistortive (AFD) phase (see Fig. 1). Many of the interesting properties of STO, either in bulk or in superlattices formed with other metal oxides, are believed to be caused by the cubic to AFD phase transition. Examples of this attribution are STO's superlattice's high-T_c superconductivity[4–6] and its colossal magnetoresistivity.[7] First-principles calculations (see Ref. 8 and references therein) have indicated that the strain-induced competition between octahedral rotation modes and the lattice distortion in metal oxide superlattices are behind these interesting properties. Thus, there is a considerable need[9,10] for precise theoretical calculations of the structural and electronic properties of complex oxides, as well as accurate estimation of the phase transition order parameters, to understand and eventually exploit these phenomena.

The phase transition of STO is governed by two order parameters. The primary order parameter is the rotation angle of the TiO_6 octahedra (θ). The experimentally measured[11] octahedral rotation of AFD STO is 1.4° at 77 K and increases as the temperature drops toward the maximum measured value of 2.1° at 4.2 K. The octahedron's rotation is believed to be almost complete[12] at around 50 K, where $\theta = 2.01° \pm 0.07°$ was reported.[13] The secondary order parameter is the tetragonality of the unit cell (c/a), which increases from 1.00056 (Ref. 14) to 1.0009 (Ref. 15) as the temperature decreases from 65 to 10 K.[16] The AFD phase can also appear in thin films of STO (Refs. 17–19) at much higher T_c than the bulk, depending on the substrate used, the thickness of deposited STO film, the strain, and the lattice mismatch. For example, 10 nm of STO deposited on $LaAlO_3$ undergoes a transition to the AFD phase at $T_c \cong 332$ K.

As the simplest metal oxide perovskite, STO has been extensively studied in recent decades with different *ab initio* schemes.[20–24] However, it is still a challenging material for theory; only a few of the previously published works have been able to accurately describe the structural and electronic properties of both phases of STO. The balance of this section will consist of a brief review of the theoretical work performed to date.

Sai and Vanderbilt[25] carried out one of the first local density approximation (LDA) calculations on STO using a plane-wave basis and ultrasoft pseudopotentials. The LDA predicted an exaggerated tetragonal AFD phase of STO, with octahedral rotation angles of 6°, significantly overestimating the 2.1° rotation measured experimentally.[11] Use of the LDA with other basis sets[26] shows similar issues, predicting rotations up 8.4°.

Wahl *et al.*[23] used a plane-wave basis while simulating STO with the LDA,[27] the Perdew-Burke-Ernzerhof (PBE) functional,[28,29] and its reparametrization for solids, PBEsol.[30,31] (See Sec. II for further descriptions of these density functionals.) The LDA underestimated experimental lattice constants, while PBE overestimated them; both methods had band gaps that were seriously underestimated compared to experiment. This underestimation is well known for these functionals; see, e.g., Ref. 32 and references therein. PBEsol was found to reproduce accurately the experimental structure, but considerably underestimated the band gaps. For the AFD phase, the octahedral angle θ was found to be very sensitive to the functional used; all three overestimate the AFD deformation, with the LDA worse than the PBE and the PBEsol splitting the difference. Rondinelli and Spaldin[33] applied the LSDA + U correction to cubic STO and found that while it corrects the band gap, the calculated octahedral

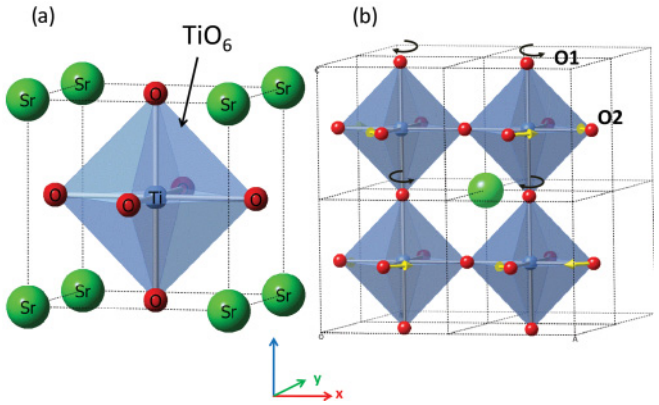

FIG. 1. (Color online) $SrTiO_3$ unit cells for the (a) cubic and (b) antiferrodistortive phases; (b) shows the TiO_6 octahedra's rotation around the [001] axis. The O_1 (equatorial) and O_2 (axial) labels denote the nonrotating and rotating oxygens, respectively.

rotation angle remains overestimated at 5.7°. To date, none of the post-DFT corrections which benefit band gaps have successfully corrected the octahedral rotation overestimation, and many authors attribute this to the argument proposed by Sai and Vanderbilt[25] stating that this can be caused by the exchange and correlation terms in DFT not capturing quantum point fluctuations.

Piskunov *et al.*[34] conducted one of the most complete and comprehensive *ab initio* studies of STO, using Gaussian basis sets specifically optimized for modeling STO crystals. This study of STO showed problems when modeling with pure DFT or pure Hartree-Fock (HF) theory, namely, underestimated and overestimated band gaps, respectively; this is a well-known problem.[35] Hybrid functionals, specifically B3PW (Ref. 36) and B3LYP (Ref. 37), gave more reasonable results, with direct band gaps overestimated by 5% for B3PW and 3.5% for B3LYP compared to experiment and indirect band gaps overestimated by 12% for B3PW and 10% for B3LYP. (We will demonstrate that an important part of this overestimation can be attributed to the basis set employed; see Sec. III.) The hybrid functionals also gave the best agreement with experiment for the lattice constant and the bulk modulus, and generally did better than semilocal functionals in all categories. This success of hybrid functionals motivated more detailed calculations[20–22,38] of the properties of the cubic and AFD phases of STO and its defects, again using the optimized basis set of Piskunov *et al.*[34] and the B3PW functional.

Next, Wahl *et al.*[23] applied the Heyd-Scuseria-Ernzerhof[39,40] (HSE) screened Coulomb hybrid density functional in a plane-wave basis set. HSE performed exceptionally well, doing much better than any of the semilocal functionals, as it gave a very accurate estimate of both the structural and electronic properties of the cubic phase. HSE also showed excellent agreement with the experimental octahedral angle and tetragonality of the unit cell which constitute, to our knowledge, the most accurately computed STO properties available in the literature for both phases, prior to the current study.

Recently, Evarestov *et al.*[24] used PBE and the hybrid functionals B3PW and the PBE0 to study the two phases of SrTiO3 using both plane-wave (PW) and linear combination of atomic orbitals (LCAO) basis sets. They found that the atomic and electronic and phonon properties calculated with PBE0 and plane waves are very similar to those published by Wahl *et al.*[23] using HSE. In addition, PBE0 phonon frequencies with both LCAO and PW basis sets are in better agreement with experiment than those obtained with PBE.

As noted above, hybrid functionals have proved their effectiveness in studying metal oxides, but they are computationally much more demanding than semilocal functionals. While it would be ideal to do high-accuracy *ab initio* calculations on metal oxide superlattices using complete basis sets and large supercells, this is prohibitively expensive at the current level of computer power. Screened hybrid functionals with only short-range exact exchange are computationally less demanding; they allow the use of large supercells, especially when used with localized basis sets such as Gaussian functions. We hope to use the most effective methods and basis sets from this study on more complicated metal oxide systems, and thus we have concentrated on methods and basis sets that would be practical for those systems as well as the systems currently under consideration.

This paper focuses on two tightly linked problems. We are interested in the degree of completeness (or size) of the localized basis set necessary to correctly simulate both phases of STO, and in the efficacy of recently developed functionals (including screened hybrids) in predicting the properties of STO. To discuss these issues, the paper proceeds as follows: In Sec. II, we briefly describe the technical details before turning in Sec. III to the basis set optimization and modification technique we used to make standard basis sets compatible with periodic boundary condition code. In Sec. IV, we report the results of semilocal and range-separated hybrid functionals applied to the cubic and the AFD phases of STO. We show also how the quality of the basis set affected the accurate prediction of the octahedral rotation angle in the AFD phase of STO. Finally, we discuss the results of our best functional and basis set combination for STO, comparing them with previously published theoretical and experimental data, with special emphasis on the effect of varying the range separation parameter in the screened functionals.

II. COMPUTATIONAL DETAILS

All calculations were performed using a development version of the GAUSSIAN suite of programs,[41] with the periodic boundary condition[42–44] (PBC) code used throughout. A wide array of functionals were applied, including the local spin density approximation[27] (LSDA), the generalized gradient approximation (GGA) corrected functional of Perdew, Burke, and Ernzerhof[28,29] (PBE), the reparametrization of PBE for solids, PBEsol,[30,31] the revised meta-GGA of Tao, Perdew, Staroverov, and Scuseria[45,46] (revTPSS), and finally a modern and highly parametrized meta-GGA functional, M06L.[47,48] Two screened hybrid functionals were also tested, namely, the short-range exact exchange functional of Heyd, Scuseria, and Ernzerhof[39,49] (HSE, with the 2006 errata, also referred to as HSE06) and the functional[50] with exact exchange in the middle range of Henderson, Izmaylov, Scuseria, and Savin (HISS).[51,52] Because regular hybrids with unscreened exact exchange like B3LYP and B3PW have higher computational

cost compared to screened hybrids we decided to exclude them from our study.

Gaussian basis sets of different quality have been tested for their ability to simulate the properties of STO; the details of these tests and the modification of the basis set were detailed enough to merit their own section, Sec. III.

A few numerical considerations should be mentioned here. During the initial (or exploratory) calculations for the AFD phase, we found some dependence of octahedral rotation angle (θ) on initial atomic positions. After further investigation, this can be attributed to the geometric optimization convergence criteria. Since θ is so small, very stringent convergence criteria are required.[53] Another modified (versus the default) setting was that a pruned integration grid for DFT of (99,590) was employed, which corresponds to the Gaussian option "ultrafine." Note that this grid is big enough for this system to avoid any of the instabilities with M06L reported in the literature with small grids.[54,55] To ensure this, we tested M06L with a larger grid, without noticing any modification in the calculated properties. Thus while "ultrafine" is sometimes insufficient for M06L, it is not for this system. Other numerical settings in GAUSSIAN were left at the default values, e.g., integral cutoffs, k-point meshes,[56] self-consistent field (SCF) convergence criterion,[57] and the like.

Finally, the geometry of each phase is worth discussing briefly. The starting configuration for the cubic phase [see Fig. 1(a)] consisted of the perovskite primitive cell containing five atoms at the experimental lattice constant[58] ($a_0 = 3.890$ Å). For the AFD phase, we could not simply use the five-atom tetragonal unit cell with rotated oxygens and the lattice parameters set to $a = b \neq c$. A 20-atom supercell/simulation cell was necessary, as the phase transition requires a rotation of every pair of neighboring TiO_6 octahedra in opposite directions [Fig. 1(b)]. Thus, the volume of the AFD supercell is about four times the volume of the cubic phase with tetragonal lattice constants $a^* = b^* = \sqrt{2}a$ and $c^* = 2c$, with a and c being the lattice parameters of the five-atom tetragonal unit cell in the AFD phase. The starting AFD structure of STO was taken from the experimental structure of Jauch and Palmer[12] obtained at 50 K and downloaded as a CIF file from the ICSD,[59] with $a^* = b^* = 5.507$ Å and $c^* = 7.796$ Å. The starting rotation angle for TiO_6 octahedra was 2.1° while $c/a - 1 = 10 \times 10^{-4}$. Please note that the geometries were only starting points; as mentioned above all geometries were optimized with the method and basis set under consideration. In order to avoid introducing any errors coming from size effects or k-space integration, the calculated properties of the AFD supercell are always compared with a 20-atom supercell constructed from four cubic primitive cells (without octahedral rotation or tetragonality) fully relaxed using the same k-point mesh. It should be noted that the supercell in the cubic phase is a local minimum and is higher in energy than the supercell in the AFD phase for all reported calculations. The final (reported) θ values were determined from Ti-O_2-Ti angle measurements, and any octahedral tilts can be estimated by measuring the Ti-O_1-Ti angles (the O_n's subscript was defined in Fig. 1). Finally, all geometric visualization was done using GAUSSVIEW.[60]

III. BASIS SET EFFICIENCY FOR $SrTiO_3$

The challenge in selecting a basis set is always balancing accuracy with computational cost. In molecular calculations, the computational cost of a Gaussian basis set is determined by the number of functions used, while in PBC calculations the spatial extent or diffuseness of the basis set also plays a major role. The more diffuse a basis set is, the larger the chunk of matter that must be included in the calculations to avoid numerical issues.

Coupled with the argument that the long density tail is more necessary for molecular work than work in extended systems, it becomes obvious that basis sets developed for nonperiodic calculations can require modification for PBC use. This section describes the basis set optimization and modification procedure we employed to find the appropriate Gaussian basis sets to simulate periodic STO while keeping within reasonable computational expense. We based our evaluations of a basis set's accuracy on cubic STO results using the Heyd-Scuseria-Ernzerhof[39,40] screened Coulomb hybrid density functional (HSE06).[49]

The obvious starting point was the basis sets used in previous calculations and studies of bulk STO, including the following:

(a) Gaussian-type basis sets published by Piskunov *et al.*[61] in 2000, optimized using the Hartree-Fock and density functional theories with Hay-Wadt pseudopotentials[62–64] for Sr and Ti, denoted here as **P1**.

(b) The subsequently improved version of **P1** published by Piskunov *et al.*[34] in 2004, which expands **P1** by adding polarization d functions to oxygen and making the Ti s and p functions more diffuse, denoted here as **P2**.

Tests on **P1** and **P2** were done with HSE06, because it has been found to give the best results versus experiment for both structural and electronic properties[23] in older calculations. Both **P1** and **P2** reproduce the experimental equilibrium lattice constants[58] (see Table I) almost perfectly. Cubic STO modeled with **P1** has a slightly higher bulk modulus compared to **P2**, although the difference between the two basis sets is fairly minimal for structural properties. A more important effect is observed for the electronic properties: **P1** and **P2** overestimate the direct band gap of STO by 0.12 and 0.05 eV, respectively, and seriously overestimate the indirect band gap by 0.28 and 0.21 eV.

TABLE I. The electronic and structural properties of cubic $SrTiO_3$ computed with HSE06 (Ref. 49) and different basis sets. Please see the text for basis set naming conventions.

Basis set	P1	P2	SZVP	TZVP	Experiment
Direct gap (eV)	3.87	3.80	3.59	3.59	3.75[a]
Indirect gap (eV)	3.53	3.46	3.18	3.20	3.25[a]
a_0 (Å)	3.900	3.908	3.887	3.902	3.890[b], 3.900[c]
B (GPa)	198	194	204	193	179[b], 179 ± 4.6[d]

[a]Reference 65.
[b]Reference 58.
[c]Reference 66.
[d]Reference 67.

It is easy to see that the **P2** basis set employed with HSE06 leads to results that are closer to experiment than **P1**, a fact noted by Piskunov *et al.*[34] for a number of functionals. The more important point is that increasing the size and quality of the basis set made a noticeable change in the results; the immediate question is whether another increase in basis set size would bring about similar improvement. In other words, using polarization *d* orbitals for O and diffuse functions for Ti improved the HSE06 results, and implies that further improvement could potentially be achieved if more basis set improvements are implemented, e.g., including titanium core electrons and/or adding more diffuse functions for oxygen.

We decided to optimize some of the **Def2-** (Ref. 68) series of Gaussian basis sets for use in bulk STO calculations. The original **Def2-** basis sets for the atoms of interest in this project included small-exponent diffuse functions ($\alpha_{\min}$ less than 0.10) that are spatially quite extended; as stated above, this long tail is necessary to improve the DFT results for molecules but not necessary for crystals.[69,70] Basis sets with large spatial ranges dramatically slow down the calculation of Coulomb contributions to the total energy of crystals. Thus, to be useful in PBC calculations, **Def2-** basis sets must be modified by removing some of the most diffuse functions.

The series of **Def2-** basis sets are available up to quadruple ζ valence (QZV) quality for a large set of elements.[68,71] In the original optimizations, the oxygen, strontium, and titanium basis sets were optimized (using HF and DFT) versus the properties of SrO, TiO, and TiO_2 molecules. Strontium has the inner-shell electrons replaced with small-core pseudopotentials,[72] while the other two atoms utilize all electron basis sets; this differs from **P1** and **P2** which use pseudopotentials on titanium as well. In general, **Def2-** basis sets are larger and more expensive than **P1** and **P2** basis sets, but are expected to give a better representation of both phases of STO due to greater "completeness."

To make a **Def2-** basis set applicable to PBC, the first step is selecting a maximum allowable diffuseness, or equivalently the smallest acceptable Gaussian orbital exponent $\alpha_{\min}$. The larger the value of $\alpha_{\min}$, the faster the calculations become, but if $\alpha_{\min}$ is set too high, significant degradation of physical property prediction results. After the threshold is defined, one pass is made through the basis set to reset all $\alpha < \alpha_{\min}$ to $\alpha_{\min}$, and then a second pass is made through the basis set to remove any redundancies. Note that after modifying or deleting an element of a contracted basis set, we rely on the internal renormalization code, i.e., no attempt is made to reoptimize contraction coefficients.

We first began with the largest **Def2-** basis sets, Def2-QZVP and Def2-QZVPP, where P and PP denote number of polarization functions added, but these were found to be computationally intractable for bulk STO even for $\alpha_{\min}$ as big as 0.2, and previous experience has shown that $\alpha_{\min}$ larger than 0.2 causes physically unacceptable results. We then moved to the smaller basis sets Def2-TZVP and Def2-SZVP. We first set $\alpha_{\min} = 0.12$, but found this made the calculations very slow. Our tests showed that $\alpha_{\min} = 0.15$ constitutes a more computationally efficient choice without important loss in accuracy.

Henceforth, the Def2-TZVP and Def2-SZVP, with $\alpha_{\min}$ modified and redundant *s* functions removed, will be denoted **TZVP** and **SZVP**, respectively.

Table I summarizes the calculated electronic and structural properties of cubic STO using our basis set modifications as well as the aforementioned **P1** and **P2**. The optimized basis sets **SZVP** and **TZVP** give an overall excellent agreement with experiment:[58] direct band gaps are now underestimated by 0.16 eV while indirect band gaps are now underestimated by ~0.05 eV. These two new basis sets are larger than the previously utilized **P1** and **P2**, are more accurate for indirect gaps, as well for other measured properties, and due to their greater size are expected to be closer to the upper limit of HSE06 accuracy for this system. Note also that the electronic properties of STO remain almost unchanged by moving from a **SZVP** to a **TZVP** basis set. The deviations from the experimental lattice constant do not exceed 0.07% and 0.3% for **SZVP** and **TZVP**, respectively, but are more substantial for the bulk modulus, reaching 14% for **SZVP** and 8% for **TZVP**. Finally, the same series of basis set optimizations were also performed using HISS and M06L functionals, which lead to the same conclusions regarding the basis set efficiency; these are not presented here for space reasons.

Before moving on to the Results section, a brief mention of the expense of the various basis sets should be included. In terms of relative CPU time, one SCF cycle takes about 12 units for **TZVP** compared to 6 units for **SZVP** and 1 unit for **P2**. All of these basis sets still have potential uses; **SZVP** or **P2**, for example, might be very useful for a rapid investigation of the electronic properties of some complex STO systems. But, in terms of completeness, **TZVP** is the most complete and the closest to the plane-wave basis set limit, followed by **SZVP**, then **P2**.

IV. RESULTS: BASIS SET AND FUNCTIONAL EVALUATION

In this section we present the calculated properties of $SrTiO_3$, always discussing the results of each functional using the **TZVP** basis set first, followed with a discussion of the sensitivity of the functionals to smaller basis sets, namely, **SZVP** and **P2**.

A. Structural properties of cubic $SrTiO_3$

The calculated equilibrium lattice constants and the bulk moduli of cubic STO obtained using different functionals and basis sets are reported in Table II. Unless otherwise specified, the deviation of theory from experiment will always be versus the data of Abramov *et al.*, i.e., that work shall be treated as the target values. Focusing first on the **TZVP** results, we observe that the screened hybrids HSE06 and HISS give lattice parameters in excellent agreement with experiment.

The calculated bulk modulus using HSE06 is fairly close to the experimentally reported values, although overestimated by 8%. (The same magnitude of overestimation has also been reported in the HSE and PBE0 plane-wave calculations of Refs. 23 and 24, respectively.) However, a larger bulk modulus overestimation of 15% is observed for HISS, which constitutes the largest deviation from experiment among all the studied functionals.

M06L and revTPSS predict slightly higher equilibrium lattice constants than do screened hybrids, but their bulk

TABLE II. Computed lattice parameter a_0 (Å) and bulk modulus B (GPa) for cubic STO using different combinations of functionals and basis sets, compared to experiment.

	HSE06	HISS	M06L	revTPSS	LSDA	PBE	PBEsol	Experiment
a_0 (Å)								3.890[a], 3.900[b]
TZVP	3.902	3.883	3.925	3.921	3.862	3.941	3.897	
SZVP	3.887	3.869	3.909	3.903	3.845	3.924	3.881	
P2	3.908	3.891	3.930	3.920	3.870	3.946	3.903	
B (GPa)								179[a],
TZVP	193	206	187	180	201	169	184	179 ± 4.6[c]
SZVP	204	218	198	193	214	180	196	
P2	194	205	191	184	203	173	187	

[a]Reference 58.
[b]Reference 66.
[c]Reference 67.

moduli are closer to experiment, with revTPSS being especially close. The LSDA underestimates the lattice constant by 0.03 Å, while PBE predicts lattice constants 0.05 Å larger than experiment. PBEsol is in excellent agreement with the experimental lattice constant. Thus PBEsol corrects the LSDA underestimation and the PBE overcorrection to LSDA for lattice constants; in addition, the PBEsol bulk modulus deviates by less than 3% from experiment, while the LSDA and PBE are off by 11% and 12%, respectively. This is an example of PBEsol meeting its purpose, as it improves the PBE lattice constant and bulk modulus for the cubic phase, approaching very closely the experimental data.

Turning now to the functional sensitivity to basis set size, we observe from the HSE06 results that the **SZVP** basis set predicts bond lengths that are very slightly shorter than the **TZVP** and a bulk modulus that is 6% higher. As such, **SZVP** predicts $SrTiO_3$ to be 14% harder than experiment. **P2** behaves in the opposite direction, predicting slightly longer bonds when compared to **TZVP**, while the bulk moduli are only 1 GPa higher. From Table II, this sensitivity of HSE06 to the smaller basis set can be generalized to M06L, revTPSS, and the semilocal functionals LSDA, PBE, and PBEsol.

Finally, it should be noted that PBEsol results offer the best agreement with experimental structural properties[58] of $SrTiO_3$ among all the studied functionals with the **TZVP** basis set, followed by the screened hybrid HSE06 and the meta-GGA revTPSS.

B. Electronic properties of cubic $SrTiO_3$

The computed electronic properties of $SrTiO_3$ are summarized in Table III. As expected, HSE06 gives an excellent estimate of the electronic properties when used with the large **TZVP** basis sets. Deviations from the experimental values are 0.16 eV for the direct gap and 0.05 for the indirect gap. A cursory glance over the rest of Table III indicates that no other functional was comparable to HSE06's efficacy for band gaps, i.e., everything else we tried had much larger errors.

The middle-range-screened hybrid HISS tends to overestimate the direct and indirect band gaps by 0.35 and 0.73 eV, respectively. M06L and revTPSS tend to underestimate both band gaps, by an average of ∼1.2 and ∼1.4 eV, respectively. The semilocal functionals LSDA, PBEsol, and PBE underestimate the experimental band gaps by an average of 45% or 1.5 eV. This was expected, and is in agreement with the behavior observed earlier in the literature for this system.[23] It can be easily seen from these results that HSE06 is the best functional choice for investigating this system.

Turning to basis set sensitivity, it can be seen from the HSE06 numbers that band gaps are nearly unaffected by using the smaller **SZVP** basis sets, but when used with the still smaller **P2** basis set, direct and indirect band gaps increase by ∼0.25 eV versus **TZVP**. The predicted direct band gap becomes closer to experiment when using **P2** and HSE06, probably due to a cancellation of errors effect, while the indirect band gap is noticeably worse. This same sensitivity holds for almost every other functional, with **SZVP** and **TZVP**

TABLE III. Direct and indirect band gaps computed for Cubic $SrTiO_3$ using different basis sets and functionals compared to experiment.

	HSE06	HISS	M06L	revTPSS	LSDA	PBE	PBEsol	Experiment
Direct gap (eV)								3.75[a]
TZVP	3.59	4.39	2.51	2.24	2.08	2.11	2.10	
SZVP	3.59	4.45	2.53	2.28	2.12	2.14	2.14	
P2	3.80	4.56	2.63	2.52	2.34	2.33	2.34	
Indirect gap (eV)								3.25[a]
TZVP	3.20	3.98	2.09	1.87	1.75	1.74	1.75	
SZVP	3.18	4.03	2.10	1.89	1.76	1.75	1.76	
P2	3.46	4.22	2.24	2.17	2.04	1.99	2.02	

[a]Reference 65.

giving about the same band gaps and **P2** opening the band gaps up by a few tenths of an eV. M06L appears to be slightly less sensitive; no obvious reason for this exists.

C. Stability of the AFD phase of STO

In this section we use the various functionals and basis sets previously tested for the cubic phase to examine the stability of the AFD phase of STO. The functional and basis set combinations tested face the challenge of predicting the AFD octahedral rotation angle, θ, as well as the tetragonality parameter c/a, which as shown in Sec. I is not trivial. The performance of each functional with **TZVP** is presented, and then an analysis of the functional's sensitivity to the smaller basis sets is presented in turn.

Figure 2 shows that the screened hybrid functional HSE06 is excellent for the structural properties of AFD, as it was for the cubic phase. Both the rotation angle θ and the c/a ratio are in very good agreement with experiment. These properties are not significantly affected when **SZVP** is used, but HSE06 with **P2** predicts a very very small angle for the AFD phase, while retaining a good c/a. This is one area where **TZVP** noticeably outperforms **P2** with HSE06.

HISS and revTPSS behave like HSE06 for both **TZVP** and **SZVP**, giving a good estimate of both order parameters. However, they demonstrate a higher sensitivity to the smaller **P2** basis set and required the use of a very stringent convergence criterion to finally relax the structure back to a pseudocubic phase with $\theta \approx 0$. On the other hand, M06L predicts the AFD phase to be unstable, and relaxes to a nonrotated structure regardless of the basis set used.

The semilocal functionals LSDA, PBEsol, and PBE all overestimate the tetragonality of the AFD phase by predicting θ and c/a almost twice the size of the experimental results. The highest overestimation was observed for the LSDA, followed by PBEsol then PBE. Note that our result here is in excellent qualitative agreement with the behavior found in the plane-wave calculations of Wahl *et al.*;[23] quantitatively, however, the LSDA, PBEsol, and PBE octahedral angles with **TZVP** are 25%–30% lower than the plane-wave results[23–26] (for a detailed numerical comparison see Table IV, and Ref. 23 has additional comparison with experiment). Similar behaviors have been recently published[24,75] for LSDA and PBE calculations with finite-range numerical atomic orbitals. This indicates that localized basis sets tend to reduce the AFD octahedral rotation compared to plane waves but do not succeed in suppressing the DFT overestimation.

When used with the **SZVP** basis sets, the LSDA, PBE, and PBEsol rotation angles are larger than the **TZVP** ones. Furthermore, when LSDA, PBEsol, and PBE are used with the **P2** basis set, we observe a small and coherent reduction in the octahedral rotation angle of the AFD structure compared to **TZVP** results. This demonstrates that semilocal functionals have different degrees of sensitivity to the quality of the localized basis sets used, but the functional choice is always the more important source of error. Thus the functionals examined here will lead to exaggerated AFD θ values for all basis sets considered.

V. DISCUSSION: PHYSICAL PROPERTIES OF STO

Before talking about specific issues, there are a few general conclusions we can reach from examining the results in Sec. IV

(1) HSE06-**P2** did a good job in describing accurately the structural properties for the cubic phase as well as providing a descent estimation of the band gap. However, its failure to correctly model the structure of the AFD phase indicates that it must be abandoned as a useful combination for this and related systems.

(2) HSE06-**SZVP** has the drawback of predicting a stiffer $SrTiO_3$ in the cubic phase, although it predicts electronic properties as well as **TVZP**. It also predicts a stiffer AFD structure, but the octahedral angle and c/a parameters are very good.

(3) HSE06-**TZVP** gave the best agreement with experiment for the cubic phase and for the AFD phase. It is definitely the most reliable combination of functional and basis set among all studied variations. Thus HSE06-**TZVP** can be used with confidence on more complicated structures, as well as to understand the change in the electronic structure during the

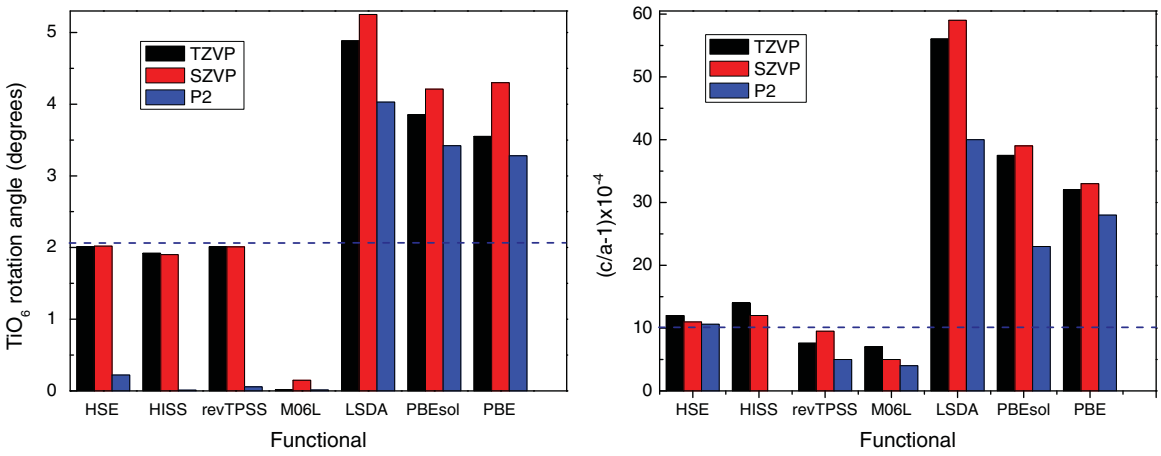

FIG. 2. (Color online) Performance of different functional and basis set combinations in predicting the order parameters of the AFD phase transition in STO. Dashed lines depict the experimental octahedral angle measured at 4.2 K from Ref. 11 (left) and the tetragonality parameter obtained at 50 K from Ref. 12 (right).

TABLE IV. Structural and electronic properties of the antiferrodistorsive phase of $SrTiO_3$ compared to previously simulated data and experiments. a^* and c^* are the lattice parameters of the AFD supercell and $c/a = c^*/\sqrt{2}a^*$. $\Delta E = E_{\text{cubic}} - E_{\text{AFD}}$ represents the gain in total energy after the cubic to AFD phase transition, while ΔE_g denotes the corresponding increase in the band gap.

	LSDA	PBE	PBEsol	HSE06	HISS	revTPSS	M06L	Experiment
a^* (Å)								
Present	5.449	5.568	5.500	5.515	5.448	5.543	5.551	5.507[f]
Ref. 23[a]	5.440	5.562	5.495	5.515				
Others		5.566[b]						
c^* (Å)								
Present	7.727	7.900	7.812	7.809	7.772	7.846	7.862	7.796[f]
Ref. 23[a]	7.755	7.897	7.818	7.808				
Others		7.908[b]						
$(c/a - 1) \times 10^{-4}$								
Present	27	32	44	12	14	7.6	7	10[f]
Ref. 23[a]	80	40	60	10				
Others	40[e]	46[b]						
θ (deg)								
Present	4.14	3.54	3.81	2.01	1.92	2.01	0	2.01 ± 0.07[f]
Ref. 23[a]	6.05	4.74	5.31	2.63				2.1[g]
Others	8.40[c],6[d] 4[e]	4.9[b]						
$\Delta E \times 10^{-5}$ (eV)								
Present	1796	854	44	35	578	258	122	
Ref. 23[a]	1900	700	1100	200				
Indirect band gap (eV)								
Present	1.820	1.787	1.808	3.227	3.995	1.890	2.060	3.246[h]
Ref. 23[a]	1.970	1.790	1.930	3.110				3.160[i]
ΔE_g (meV)								
Present	75	49	58	27	15	15	30	50[j]
Ref. 23[a]	160	10	110	40				

[a]Plane-wave calculation using a different HSE screening parameter.
[b]Reference 24, plane-wave data.
[c]Reference 26.
[d]Reference 25.
[e]Reference 75 using numerical atomic orbitals.
[f]Reference 12 (at 50 K).
[g]Reference 11 (at 4.2 K).
[h]Reference 73.
[i]Reference 74.
[j]Reference 73 difference between 85 K and 8 K measured gaps.

cubic to AFD transition for this system. More concisely, we believe that this combination is an accurate enough functional in a good enough basis set to explain phenomena in metal oxides.

A. Band structure alteration by the AFD phase transition

The band structure of the cubic unit cell of STO computed with HSE06 and **TZVP** is shown in Fig. 3, with the high-symmetry points $\Gamma = (0,0,0)$, $X = (0,\frac{1}{2},0)$, $M = (\frac{1}{2},\frac{1}{2},0)$, and $R = (\frac{1}{2},\frac{1}{2},\frac{1}{2})$ labeled, in the first Brillouin zone of the simple cubic system. The dashed line depicts the Fermi level lying at the valence band maximum at the R point.

Our band structure agrees qualitatively with previous band structures from LSDA-PW calculations, which can be seen (for example) in Fig. 5 of Ref. 26, as well as the B3PW-**P2** band structure in Ref. 34, Fig. 2(a), with the exception of a few details. Our direct band gap ($\Gamma \rightarrow \Gamma$) of 3.59 eV and

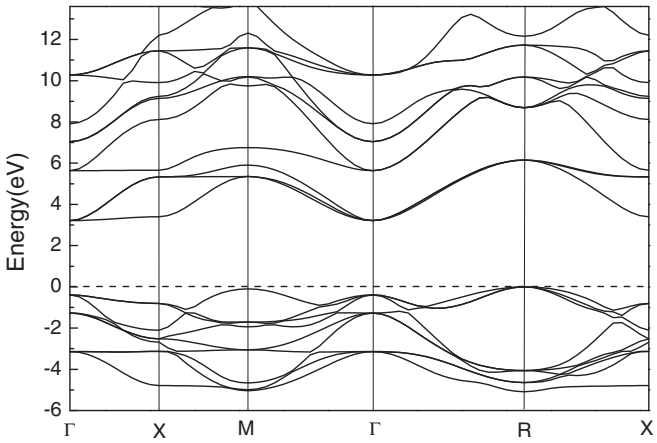

FIG. 3. Band structure of cubic $SrTiO_3$ unit cell calculated with HSE06 and **TZVP**. The dashed line depicts the Fermi level lying at the valence band maximum (R special point.)

indirect gap ($R \rightarrow \Gamma$) of 3.2 eV are in better agreement with experiment[65] compared to the underestimation observed in the LSDA-PW gaps and the overestimation found with B3PW-**P2**. Thus for a DFT approach, this diagram is the best band structure to date to our knowledge. [An even more accurate band structure was computed using the experimental lattice constant of $SrTiO_3$ by mean of a post-LSDA quasiparticle self-consistent GW (QSGW) correction to the band structure by Hamann and Vanderbilt.[76]]

Figure 4 shows the total density of states (DOS) of the unit cell as well as the projected density of states (PDOS) on every atomic orbital. The PDOS of oxygen represents the sum of the contributions of all three oxygen atoms in the cubic unit cell. In the energy window shown here, the DOS is dominated by oxygen $2p$, titanium $3d$, and strontium $4d$ states. (All the remaining orbitals have a negligible contribution, so their PDOSs are not shown.) The valence band (VB) from 0 to -6 eV is dominated by oxygen $2p$ states, with a small contribution from titanium $3d$ states in the range -3 to -6 eV. The conduction band (CB) is clearly dominated by titanium $3d$ in the energy range 3.2–7 eV, with a smaller contribution coming from the three oxygen $2p$ states as well. The admixture in the VB and CB between the titanium $3d$ and oxygen $2p$ orbitals demonstrates that the Ti–O bonds have a partially covalent character with a small degree of hybridization. (This behavior has been noted in previously published data.[26]) Between 7 and 9 eV, the spectrum is the sum of contributions from oxygen $2p$, titanium $3d$, and strontium $4d$ orbitals. The higher-energy region in the CB (9–12 eV) is dominated by strontium $4d$ orbitals with small contributions from titanium $3d$ and with oxygen $2p$ vanishing at around 10.5 eV.

Figure 5 compares the total electronic densities of states for the cubic and AFD supercells. As a general trend, the cubic to AFD phase transition does not lead to a significant modification in the total DOS; both the valence and the conduction bands experience a slight shift to higher energies together with some small modifications. However, the VB shift does not affect the peak at the VB maximum, while a very small shift to higher energies is observed for the CB minimum, indicating that the band gap increase by ≈27 meV after the transition. This same behavior holds for all the functional and basis set combinations tested, and is in line with some experimental observations[74] reporting very small changes in their measured band gaps due to the cubic to tetragonal structural transition. Further confirmation of this physical effect can be seen in recent photoluminescence measurements,[73] which reported that the band gap increased by 50 meV when the temperature decreased from 85 to 8 K, which is a temperature range over which the AFD rotation would go from incomplete to nearly total.

A more detailed comparison between the PDOS for each atomic orbital can give a better understanding of the origin of these modifications (see Fig. 5). It is important to mention that in the AFD supercell, there is one nonrotating O_1 atom and two rotating O_2 oxygens for every Sr and Ti atom. Concentrating on the oxygen $2p$ orbitals, we observe that the nonrotating O_1 atoms are nearly unchanged in the PDOS compared to the cubic phase, with the exception of a tiny shift to higher energy (not shown here for sake of simplicity), which can be attributed to the elongation of the cell along the z axis. However, the O_2 demonstrate a much more significant shift to higher energies, along with changes in the height and width of some peaks. This is mainly caused by the octahedral rotation involving O_2 atoms. The titanium $3d$ and strontium $4d$ spectra experience the same aforementioned shift to higher energies in the VB and the CB due to the elongation of the lattice, with a few noticeable changes in the titanium $3d$ spectrum at -2.9 as well as between 5 and 6.5 eV. Most of the modifications observed in the total DOS, with the exception of a few, originate from the changes in the O_2 $2p$ and Ti $3d$ spectra with the O_2 being far more important.

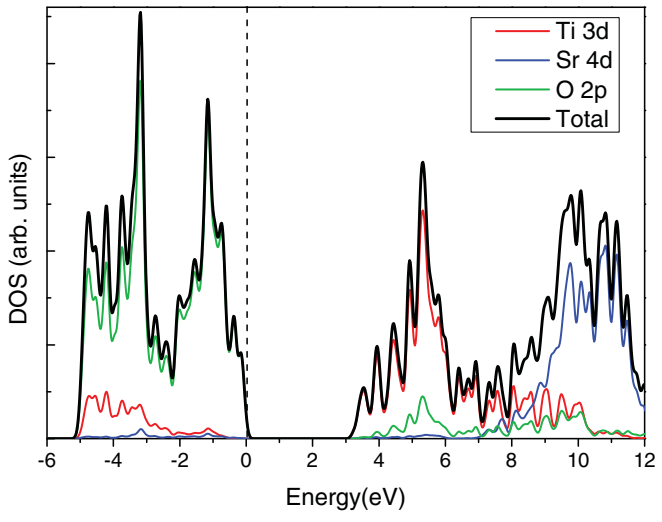

FIG. 4. (Color online) Total electronic density of states (DOS) of cubic $SrTiO_3$ unit cell calculated with HSE06 and **TZVP**. Projected densities of states (PDOSs) of the main contributing atomic orbitals are also shown.

B. The effect of the HSE screening parameter ω

Relying on the assumption that plane waves are much closer to the infinite basis set limit than the Gaussian basis sets we used, it is useful to compare our HSE06-**TZVP** results with the HSE plane-wave results. To our knowledge, only Wahl *et al.*[23] have published data using plane waves and a Heyd-Scuseria-Ernzerhof[39,40,49] style screened Coulomb hybrid density functional for this system. However, a direct comparison with our present data is not possible because Wahl *et al.* used a different screening parameter in their calculations.

Briefly, the HSE functional partitions the Coulomb potential into short-range (SR) and long-range (LR) components:

$$E_{xc}^{\mathrm{HSE}} = \tfrac{1}{4} E_x^{\mathrm{HF,SR}}(\omega) + \tfrac{3}{4} E_x^{\mathrm{PBE,SR}}(\omega) + E_x^{\mathrm{PBE,LR}}(\omega) + E_c^{\mathrm{PBE}}. \quad (1)$$

The screening parameter ω defines the separation range, as it controls the distance at which the long-range nonlocal interaction becomes negligible, i.e., it "turns off" exact exchange after a specified distance. Wahl *et al.* used $\omega_1 = 0.159$ a.u.$^{-1}$, effectively using an HSE-style functional, but not either of the functionals HSE03 or HSE06.[77] Krukau *et al.*[49] applied HSE while varying ω in the range $0.11 \leqslant \omega \leqslant 0.20$ to a

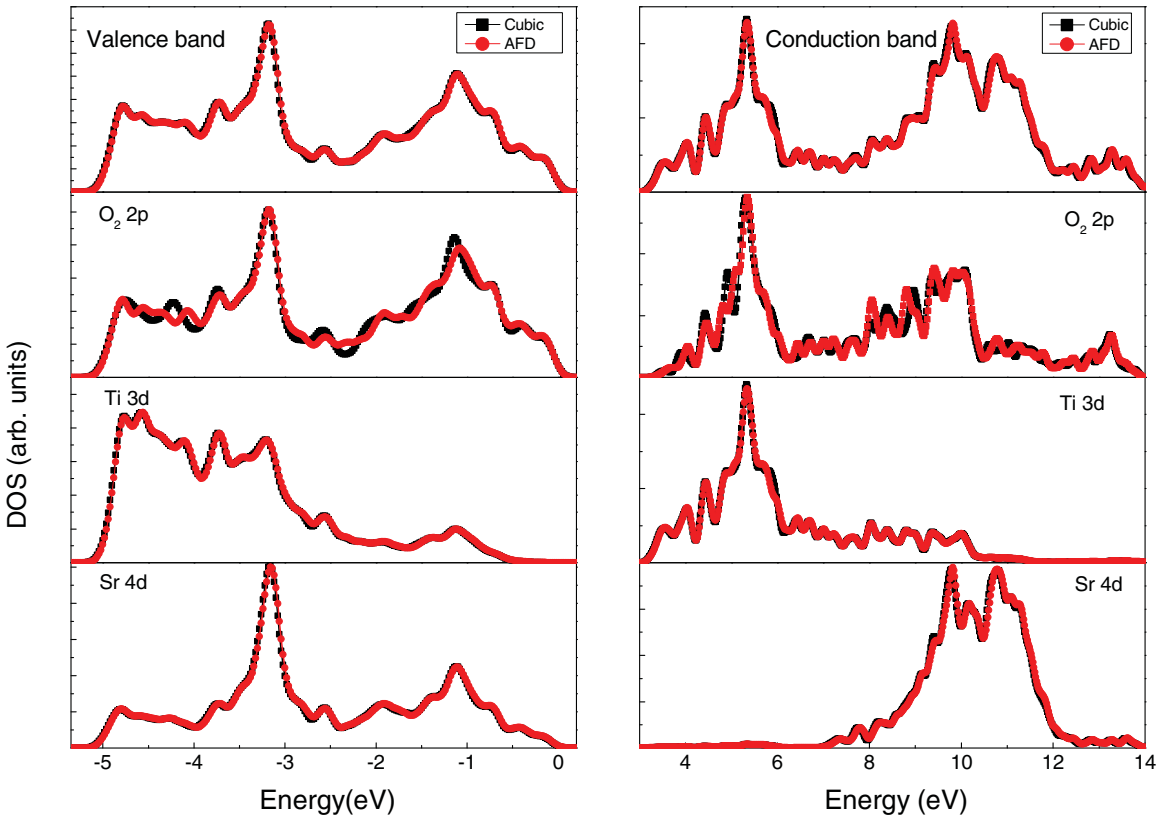

FIG. 5. (Color online) Modification in the total and partial atomic electronic densities of states of $SrTiO_3$ upon the cubic to AFD phase transition.

number of bulk metals and semiconductors. They concluded that a small increase of ω substantially lowers the calculated band gaps and the smaller the value ω takes in this range, the closer the calculated band gaps and lattice constants are to the experiment. Based on the above, Krukau *et al.*[49] recommended $\omega_2 = 0.11$ a.u.$^{-1}$ for both the HF and PBE parts of the exchange. This is the value we used in all our calculations, and this value is part of the formal definition of HSE06. However, in order to make a comparison between our HSE(ω_2)-TZVP and the HSE(ω_1)-PW data of Wahl *et al.*, we must perform a HSE and TZVP calculation with ω_1 and isolate the screening parameter effect on the calculated properties of $SrTiO_3$.

Table V shows that the HSE(ω_1)-TZVP lattice constant and bulk modulus change very slightly on decreasing the screening parameter from ω_1 to ω_2: the changes are 0.001 Å and 1 GPa, respectively. A much more significant effect is, however, observed for the band gaps: decreasing the screening parameter by 50% ($\omega_1 \rightarrow \omega_2$) leads to an increase in the band gaps, effectively a rigid shift of 0.22 and 0.24 eV for the direct and indirect band gaps, respectively. If examined from the other direction, decreasing the screening parameter from ω_1 to ω_2 (with HSE and **TZVP**) tends to bring the band gaps closer to the experiment (see Table V), which suggests that ω_2 provides better agreement with experiment than does ω_1. The same structural changes and band gap shifts were also found for the small basis sets **SZVP** and **P2**, which are not presented here and which demonstrate that this effect is completely independent of the basis set used. Finally, the HSE(ω_2)-TZVP band gaps are very close to the HSE(ω_2)-PW values we estimated, suggesting that our **TZVP** basis set is very close in quality to the previously used plane waves, and thus is closer to the basis set limit.

This section contains one of the most important results of this paper, which as such should be clearly restated. If we use the same version of HSE used in plane-wave studies, we can show that our **TZVP** is a high-quality basis set as it matches the excellent plane-wave results. If we use the proper

TABLE V. Variation of the cubic STO lattice parameter (a_0 in Å), bulk modulus (B in GPa), and direct (E_g^d) and indirect (E_g^i) band gaps (in eV) on decreasing the HSE screening parameter from $\omega_1 = 0.159$ a.u.$^{-1}$ to $\omega_2 = 0.11$ a.u.$^{-1}$. Results are from our Gaussian basis set (**TZVP**) and the plane-wave (PW) calculations in Ref. 23.

	Gaussian		PW		
	$\omega_1 \longrightarrow \omega_2$		$\omega_1 \longrightarrow \omega_2$		Experiment
a_0	3.903	3.902	3.904	3.903[e]	3.890[a], 3.900[b]
B	192	193	192	193[e]	179[a], 179±4.6[c]
E_g^d	3.37	3.59	3.47	3.67[e]	3.75[d]
E_g^i	2.96	3.20	3.07	3.27[e]	3.25[d]

[a]Reference 58.
[b]Reference 66.
[c]Reference 67.
[d]Reference 65.
[e]Estimated values if $\omega_2 = 0.11$ a.u.$^{-1}$ was used in plane-wave calculations of Ref. 23.

TABLE VI. Our most converged direct (E_g^d) and indirect (E_g^i) band gaps (in eV) for cubic STO alongside previously published hybrid functional results done with the **P2** basis set. Original regular hybrid data (Ori) and the corrected data (Corr) according to the basis set sensitivity effect deduced in Sec. IV B.

		E_g^d		E_g^i	
	Functional/basis	Ori.	Corr.[estimated]	Ori.	Corr.[estimated]
Expt. (Ref. 65)		3.75		3.25	
Present	HSE06/**TZVP**	3.59		3.20	
Ref. 34	B3PW/**P2**	3.96	3.74	3.63	3.35
	B3LYP/**P2**	3.89	3.67	3.57	3.30
Ref. 78	B3PW/**P2**	4.02	3.80	3.70	3.42
Ref. 20	B3PW/**P2**	–	–	3.63	3.35
Ref. 79	B1-WC/**P2**[a]	3.91		3.57	

[a]**P2** basis set with all electrons for Ti; basis set correction cannot be applied.

ω in HSE with our basis set, we arrive at the best results and smallest errors versus experiment ever reported for $SrTiO_3$, to our knowledge.

Finally, it should be noted that this is not an *ad hoc* parametrization of ω to give the best results for this study. We were able to obtain results that closely match experiment by using a demonstrably high-quality basis set and a parameter in the density functional determined by a large test bed of structures and properties.[49]

C. Screened hybrids compared to regular hybrids

Table VI summarizes the calculated band gaps of HSE06 with **TZVP** and compares them with previously published gaps computed with the regular hybrids B3PW and B3LYP, done with the **P2** basis set. There are noticeable differences between the results of HSE06 and the regular hybrids, with HSE06-**TZVP** giving band gaps very close to experiment while regular hybrids used with **P2** overestimate the gap, especially the indirect band gap. The band gap overestimation is of the same magnitude as we observed in Sec. IV B for HSE06 with **P2** as well as all the other functionals tested on STO with **P2**. This suggests that **P2** is also behind the band gap overestimation in the regular hybrids data reported in the literature.[20,34,78] By comparing the **P2** and **TZVP** band gaps from Table III, we can deduce that the **P2** basis set has the effect (versus a large basis set) of increasing the direct and indirect band gaps by average values of 0.22 and 0.28 eV, respectively. By applying this **P2** $\rightarrow$ **TZVP** basis set correction to the regular hybrid B3PW-**P2** and B3LYP-**P2** the original band gaps (see the corrected values in Table VI), the original band gaps are brought closer to the experimental values, and thus closer to the HSE06-**TZVP** results as well. Consequently, differences in the computed electronic properties of HSE06 and B3PW and B3LYP are considerably attenuated and this suggests that the screened hybrid HSE06 is comparable in accuracy with regular hybrids for STO, while being much more computationally efficient.

The final issue to discuss is the comparison of the structural and elastic properties of STO computed with HSE06 versus regular hybrids. Perovskite crystals in the cubic structure have only three independent elastic constants, namely, C_{11}, C_{12}, and C_{44}, as well as a bulk modulus:

$$B = \tfrac{1}{3}(C_{11} + 2C_{12}). \quad (2)$$

We calculated the elastic constants of STO using HSE06 and **TVZP**, following the methodology described in Ref. 80. Ideally we would like to compare our cubic elastic constants calculated at 0 K with low-temperature data, but experimentally the cubic structure turns to a tetragonal structure below a transition temperature, making any comparison of this kind impossible. Experimentally, Bell and Rupprecht[81] found that the elastic constants of STO measured between 303 and 112 K obey the following empirical relations:

$$C_{11} = 334.1\left[1 - 2.62\times10^{-4}(T - T_a) - \frac{0.0992}{(T - T_a)}\right], \quad (3a)$$

$$C_{12} = 104.9\left[1 - 1.23\times10^{-4}(T - T_a) + \frac{0.1064}{(T - T_a)}\right], \quad (3b)$$

$$C_{44} = 126.7\left[1 - 1.30\times10^{-4}(T - T_a) - \frac{0.1242}{(T - T_a)}\right], \quad (3c)$$

where the elastic constants are in GPa, T is the temperature, and $T_a = 108$ K is the critical temperature. C_{11} and C_{44} reach their maximum values at 133 K where STO is still cubic, and then they start to decrease as $-1/(T - T_a)$ in the region around the transition temperature; in contrast, C_{12} continues to increase as $1/(T - T_a)$ in the same temperature range.

Since we do not know at what temperature the change from the cubic to tetragonal phase begins to take place, it is better to limit our comparison to data measured at 133 K and above. Table VII summarizes our results and compares them with experiment as well as previously published results with B3PW-**P2** and B3LYP-**P2**. HSE06-**TZVP** provides excellent lattice constants but predicts the bulk modulus to be 8% higher than experiment. The elastic constants from HSE06-**TZVP** overestimate the experimental data at room temperature by 10% and the 133 K data by 6%; this was expected given the overestimation of the bulk modulus. The B3PW hybrid also gave very good lattice constant and bulk modulus, but the

TABLE VII. Calculated elastic constants with HSE06-**TZVP** for cubic STO compared to experiment and previously published results with the regular hybrid functional B3PW and the **P2** basis set from Ref. 34. a_0 is in Å, B, C_{11}, C_{12}, and C_{44} are in GPa.

	a_0	B	C_{11}	C_{12}	C_{44}
HSE06-**TZVP**	3.902	193	351.4	113	137.3
B3PW-**P2**	3.900	177	316	92.7	120.1
B3LYP-**P2**	3.940	177	328.3	105.7	124.6
Expt.	3.890[a]	179[a]	317.2	102.5	123.5[b]
	3.900[c]	179±4.6[d]	330	105	126[e]
	3.910	184			128[f]

[a]Ref. 58
[b]Ref. 81 at room temperature.
[c]Ref. 66
[d]Ref. 67
[e]Ref. 81: maximum measured values for C_{11} and C_{44} at 133 K; C_{12} increases further as temperature drops.
[f]Ref. 82.

calculated elastic constants are lower than the room- and the low-temperature experimental values. B3LYP predicted a lattice constant higher by 1% and a good bulk modulus, and offers the best agreement with the low-temperature elastic constants. In summary, none of the screened or regular hybrids considered was able to give simultaneously excellent bulk moduli and elastic constants; still the combination HSE06-**TZVP** offers the best compromise between efficiency, accuracy, and speed.

VI. CONCLUSION

We used the *ab initio* code GAUSSIAN to simulate the properties of $SrTiO_3$ using a large spectrum of functionals, from LSDA, GGAs (PBE and PBEsol), and meta-GGAs (M06L and revTPSS) to modern range-separated hybrid functionals (HSE06 and HISS), assessing their ability in predicting the properties of the cubic and the AFD phases of STO.

We found that pure DFT functionals tend to overestimate the octahedral rotation angles of the AFD phase, in agreement with previously reported results in the literature using plane-wave basis sets of comparable quality.[23] Also, basis sets of low quality tend to inhibit the tetragonality of the AFD phase and sometimes even suppress it, regardless of the functional used. We therefore constructed a localized basis set of sufficient completeness (or size) to correctly simulate the TiO_6 octahedral rotation and the cubic phases of STO. We also evaluated the band gap errors arising from the use of the **P2** basis set and from the magnitude of the HSE screening parameter ω. By applying our basis set and ω corrections to the previously published work with regular and screened hybrid functionals on STO, we showed that the discrepancies between published simulated data can be explained and that hybrid functionals used with sufficiently big Gaussian-type basis sets can give results comparable with plane-wave calculations and in excellent agreement with experiment.

The screened hybrid functional HSE06 predicts the electronic and structural properties of the cubic and AFD phases in very good agreement with experiment, especially if used with the high-quality basis set **TZVP**. HSE06-**TZVP** is the most reliable combination of functional and Gaussian basis set for STO which is computationally tractable with the current computer power. It is accurate enough to enable us to understand the changes in the band structure during the cubic to AFD phase transition. The success of HSE06 with **TZVP** encourages its use on more complicated cases like bond breaking and overbinding and defect formation, where the basis set completeness is expected to play a major role.

ACKNOWLEDGMENTS

This work is supported by the Qatar National Research Fund (QNRF) through the National Priorities Research Program (NPRP Grant No. 481007-20000). We are thankful to Cris V. Diaconu for the technical support with the band structure code in GAUSSIAN. We are grateful to the research computing facilities at Texas A&M university at Qatar for generous allocations of computer resources.

*fadwa.el_mellouhi@qatar.tamu.edu
†ed.brothers@qatar.tamu.edu

[1] K. Ueno, S. Nakamura, H. Shimotani, A. Ohtomo, N. Kimura, T. Nojima, H. Aoki, Y. Iwasa, and M. Kawasaki, Nature Mater. **7**, 855 (2008).
[2] D. Kan, T. Tetashima, R. Kanda, A. Masuno, K. Tanaka, S. Chu, H. Kan, A. Ishizumi, Y. Kanemitsu, Y. Shimakawa, and M. Takano, Nature Mater. **4**, 816 (2005).
[3] N. Zhou, K. Zhao, H. Liu, Z. Lu, H. Zhao, L. Tian, W. Liu, and S. Zhao, J. Appl. Phys. **105**, 083110 (2009).
[4] N. Reyren, S. Thiel, A. D. Caviglia, L. F. Kourkoutis, G. Hammerl, C. Richter, C. W. Schneider, T. Kopp, A. S. Rueetschi, D. Jaccard, M. Gabay, D. A. Muller, J. M. Triscone, and J. Mannhart, Science **317**, 1196 (2007).
[5] A. D. Caviglia, S. Gariglio, N. Reyren, D. Jaccard, T. Schneider, M. Gabay, S. Thiel, G. Hammerl, J. Mannhart, and J. M. Triscone, Nature (London) **456**, 624 (2008).
[6] Y. Kozuka, M. Kim, C. Bell, B. G. Kim, Y. Hikita, and H. Y. Hwang, Nature (London) **462**, 487 (2009).
[7] G. M. Gao, C. L. Chen, L. A. Han, and X. S. Cao, J. Appl. Phys. **105**, 033707 (2009).
[8] R. Pentcheva and W. E. Pickett, J. Phys.: Condens. Matter **22**, 043001 (2010).
[9] A. Y. Borisevich, H. J. Chang, M. Huijben, M. P. Oxley, S. Okamoto, M. K. Niranjan, J. D. Burton, E. Y. Tsymbal, Y. H. Chu, P. Yu, R. Ramesh, S. V. Kalinin, and S. J. Pennycook, Phys. Rev. Lett. **105**, 087204 (2010).
[10] Y. J. Chang, A. Bostwick, Y. S. Kim, K. Horn, and E. Rotenberg, Phys. Rev. B **81**, 235109 (2010).
[11] H. Unoki and T. Sakudo, J. Phys. Soc. Jpn. **23**, 546 (1967).
[12] W. Jauch and A. Palmer, Phys. Rev. B **60**, 2961 (1999).
[13] As the standard DFT calculations reported in this paper do not include temperature, we take the 0 K experimental/target value to be 2.1°.
[14] L. Cao, E. Sozontov, and J. Zegenhagen, Phys. Status Solidi A **181**, 387 (2000).
[15] A. Heidemann and H. Wettengel, Z. Phys. **258**, 429 (1973).
[16] As temperature is not included in the standard DFT work done here, we take the 0 K experimental/target value to be 1.0009.
[17] F. He, B. O. Wells, Z. G. Ban, S. P. Alpay, S. Grenier, S. M. Shapiro, W. Si, A. Clark, and X. X. Xi, Phys. Rev. B **70**, 235405 (2004).
[18] F. He, B. O. Wells, and S. M. Shapiro, Phys. Rev. Lett. **94**, 176101 (2005).
[19] F. He, B. O. Wells, S. M. Shapiro, M. v. Zimmermann, A. Clark, and X. X. Xi, Appl. Phys. Lett. **83**, 123 (2003).
[20] Y. F. Zhukovskii, E. A. Kotomin, S. Piskunov, and D. E. Ellis, Solid State Commun. **149**, 1359 (2009).
[21] R. I. Eglitis and D. Vanderbilt, Phys. Rev. B **77**, 195408 (2008).
[22] E. Heifets, E. Kotomin, and V. A. Trepakov, J. Phys.: Condens. Matter **18**, 4845 (2006).
[23] R. Wahl, D. Vogtenhuber, and G. Kresse, Phys. Rev. B **78**, 104116 (2008).
[24] R. A. Evarestov, E. Blokhin, D. Gryaznov, E. A. Kotomin, and J. Maier, Phys. Rev. B **83**, 134108 (2011).
[25] N. Sai and D. Vanderbilt, Phys. Rev. B **62**, 13942 (2000).

[26]K. Uchida, S. Tsuneyuki, and T. Schimizu, Phys. Rev. B **68**, 174107 (2003).
[27]S. H. Vosko, L. Wilk, and M. Nusair, Can. J. Phys. **58**, 1200 (1980).
[28]J. P. Perdew, K. Burke, and M. Ernzerhof, Phys. Rev. Lett. **77**, 3865 (1996).
[29]J. P. Perdew, K. Burke, and M. Ernzerhof, Phys. Rev. Lett. **78**, 1396 (1997).
[30]V. N. Staroverov, G. E. Scuseria, J. Tao, and J. P. Perdew, J. Chem. Phys. **119**, 12129 (2003).
[31]V. N. Staroverov, G. E. Scuseria, J. Tao, and J. P. Perdew, J. Chem. Phys. **121**, 11507 (2004).
[32]P. Mori-Sánchez, A. J. Cohen, and W. Yang, Phys. Rev. Lett. **100**, 146401 (2008).
[33]J. M. Rondinelli and N. A. Spaldin, Phys. Rev. B **82**, 113402 (2010).
[34]S. Piskunov, E. Heifets, R. I. Eglitis, and G. Borstel, Comput. Mater. Sci. **29**, 165 (2004).
[35]B. G. Janesko, T. M. Henderson, and G. E. Scuseria, PhysChemChemPhys. **11**, 443 (2009).
[36]A. D. Becke, J. Chem. Phys. **98**, 5648 (1993).
[37]C. Lee, W. Yang, and R. G. Parr, Phys. Rev. B **37**, 785 (1988).
[38]V. E. Alexandrov, E. A. Kotomin, J. Maier, and R. A. Evarestov, Eur. Phys. J. B **72**, 53 (2009).
[39]J. Heyd, G. E. Scuseria, and M. Ernzerhof, J. Chem. Phys. **118**, 8207 (2003).
[40]J. Heyd, G. E. Scuseria, and M. Ernzerhof, J. Chem. Phys. **124**, 219906 (2006).
[41]M. J. Frisch, G. W. Trucks, G. E. Schlegel, H. B. Scuseria, M. A. Robb, J. R. Cheeseman, G. Scalmani, V. Barone, B. Mennucci, G. A. Petersson, H. Nakatsuji, M. Caricato, X. Li, H. P. Hratchian, A. F. Izmaylov, J. Bloino, G. Zheng, J. L. Sonnenberg, M. Hada, M. Ehara, K. Toyota, R. Fukuda, J. Hasegawa, M. Ishida, T. Nakajima, Y. Honda, O. Kitao, H. Nakai, T. Vreven, J. A. Montgomery Jr., J. E. Peralta, F. Ogliaro, M. Bearpark, J. J. Heyd, E. Brothers, V. N. Kudin, K. N. Staroverov, R. Kobayashi, J. Normand, K. Raghavachari, A. Rendell, J. C. Burant, S. S. Iyengar, J. Tomasi, M. Cossi, N. Rega, J. M. Millam, M. Klene, J. E. Knox, J. B. Cross, V. Bakken, C. Adamo, J. Jaramillo, R. Gomperts, R. E. Stratmann, O. Yazyev, A. J. Austin, R. Cammi, C. Pomelli, R. L. Ochterski, J. W. Martin, K. Morokuma, V. G. Zakrzewski, G. A. Voth, P. Salvador, J. J. Dannenberg, S. Dapprich, A. D. Daniels, O. Farkas, J. B. Foresman, J. V. Ortiz, J. Cioslowski, and D. J. Fox, GAUSSIAN development version, revision h.07+ (Gaussian, Inc., Wallingford, CT).
[42]K. N. Kudin and G. E. Scuseria, Phys. Rev. B **61**, 16440 (2000).
[43]K. N. Kudin and G. E. Scuseria, Chem. Phys. Lett. **289**, 611 (1998).
[44]K. N. Kudin and G. E. Scuseria, Chem. Phys. Lett. **283**, 61 (1998).
[45]J. Tao, J. P. Perdew, V. N. Staroverov, and G. E. Scuseria, Phys. Rev. Lett. **91**, 146401 (2003).
[46]J. P. Perdew, A. Ruzsinszky, G. I. Csonka, L. A. Constantin, and J. Sun, Phys. Rev. Lett. **103**, 026403 (2009).
[47]Y. Zhao and D. G. Truhlar, J. Chem. Phys. **125**, 194101 (2006).
[48]Y. Zhao and D. G. Truhlar, J. Chem. Phys. **128**, 184109 (2008).
[49]A. V. Krukau, O. A. Vydrov, A. F. Izmaylov, and G. E. Scuseria, J. Chem. Phys. **125**, 224106 (2006).
[50]Originally introduced as HISS-B in Ref. 51 and here called simply HISS as in Ref. 52.
[51]T. M. Henderson, A. F. Izmaylov, G. E. Scuseria, and A. Savin, J. Chem. Phys. **127**, 221103 (2007).
[52]T. M. Henderson, A. F. Izmaylov, G. E. Scuseria, and A. Savin, J. Chem. Theory Comput. **4**, 1254 (2008).
[53]The standard rms force threshold in GAUSSIAN for geometry optimizations is 450×10^{-6} hartrees/bohr. Using "verytight" convergence, this becomes 1×10^{-6}.
[54]E. R. Johnson, A. D. Becke, C. D. Sherrill, and G. A. DiLabio, J. Chem. Phys. **131**, 034111 (2009).
[55]S. E. Wheeler and K. N. Houk, J. Chem. Theory Comput. **6**, 395 (2010) [http://pubs.acs.org/doi/pdf/10.1021/ct900639j].
[56]Reciprocal space integration used $12 \times 12 \times 12$ k-point mesh for the cubic unit cell, while for the larger AFD supercell, the default k-point mesh of $8 \times 8 \times 6$ was found to be sufficient.
[57]Because we did geometry optimization, this was by default set to "tight," or 10^{-8}.
[58]Y. A. Abramov, V. G. Tsirelson, V. E. Zavodnik, S. A. Ivanov, and I. D. Brown, Acta Crystallogr. Sect. B **51**, 942 (1995).
[59][http://www.fiz-karlsruhe.de/icsd.htm].
[60]R. Dennington, T. Keith, and J. Millam, computer code GAUSSVIEW Version 5 (Semichem Inc. Shawnee Mission, KS, 2009).
[61]S. Piskunov, Y. F. Zhukovskii, E. A. Kotomin, and Y. N. Shunin, Comp. Modell. New Technol. **4**, 7 (2000).
[62]J. P. Hay and R. W. Wadt, J. Chem. Phys **82**, 270 (1984).
[63]R. W. Wadt and J. P. Hay, J. Chem. Phys. **82**, 284 (1984).
[64]J. P. Hay and R. W. Wadt, J. Chem. Phys. **82**, 299 (1984).
[65]K. van Benthem, C. Elsasser, and R. H. French, J. Appl. Phys. **90**, 6156 (2001).
[66]*Ferroelectrics and Related Substances*, edited by K. H. Hellwege and A. M. Hellwege, Landolt-Börnstein, New Series, Group III, Vol. 3 (Springer-Verlag, Berlin, 1969).
[67]G. J. Fischer, Z. Wang, and S. Karato, Phys. Chem. Miner. **20**, 97 (1993).
[68]F. Weigend and R. Ahlrichs, PhysChemChemPhys **7**, 3297 (2005).
[69]J. Heyd, J. E. Peralta, G. E. Scuseria, and R. L. Martin, J. Chem. Phys. **123**, 174101 (2005).
[70]M. C. Strain, G. E. Scuseria, and M. J. Frisch, Science **271**, 51 (1996).
[71]F. Weigend, PhysChemChemPhys **8**, 1057 (2006).
[72]M. Kaupp, P. v. R. Schleyer, H. Stoll, and H. Preuss, J. Chem. Phys. **94**, 1360 (1991).
[73]Y. Yamada and Y. Kanemitsu, Phys. Rev. B **82**, 121103 (2010).
[74]T. Hasegawa, M. Shirai, and K. Tanaka, J. Lumin. **87–89**, 1217 (2000).
[75]J. Hong, G. Catalan, J. F. Scott, and E. Artacho, J. Phys.: Condens. Matter **22**, 112201 (2010).
[76]D. R. Hamann and D. Vanderbilt, Phys. Rev. B **79**, 045109 (2009).
[77]See the first page of Ref. 40 for the difference between the HSE03 and HSE06, namely, HSE03 used $\omega_{\mathrm{HF}} = 0.15/\sqrt{2}$ bohrs^{-1} and $\omega_{\mathrm{PBE}} = 0.15 \times 2^{1/3}$ bohrs^{-1}, HSE06 uses $\omega_{\mathrm{HF}} = \omega_{\mathrm{PBE}} = 0.11$ bohrs^{-1}. HSE from Ref. 23 used $\omega_{\mathrm{HF}} = \omega_{\mathrm{PBE}} = 0.159$ bohr^{-1}.
[78]E. Heifets, E. Kotomin, and V. A. Trepakov, J. Phys.: Condens. Matter **18**, 4845 (2006).
[79]D. I. Bilc, R. Orlando, R. Shaltaf, G. M. Rignanese, J. Íñiguez, and P. Ghosez, Phys. Rev. B **77**, 165107 (2008).
[80]Z. Wu, X.-J. Chen, V. V. Struzhkin, and R. E. Cohen, Phys. Rev. B **71**, 214103 (2005).
[81]R. O. Bell and G. Rupprecht, Phys. Rev. **129**, 90 (1963).
[82]M. Adachi *et al.*, *Landolt-Börnstein-Group III Condensed Matter Numerical Data and Functional Relationships in Science and Technology*, edited by Y. Shiozaki, E. Nakamura, and T. Mitsui, Vol. 36A1: Oxides, Pt. V (Springer, Berlin, 2002), Chap. 1A, p. 11647.